

# Accelerating Deconvolution on Unmodified Deep Learning Processors for Generative Adversarial Networks A Software Approach

Kaijie Tu

*Institute of Computing Technology, Chinese Academy of Sciences, Beijing, China*

tukaijie@ict.ac.cn

**Abstract**—Generative Adversarial Networks (GANs) are the emerging machine learning technology that can learn to automatically create labeled datasets in application domains such as speech, image, video and texts. A GAN typically includes a generative model that is taught to generate any distribution of data, and a discriminator trained to distinguish the synthetic data from real-world data. Both convolutional and deconvolutional layers are the major sources of performance overhead for GANs and directly impact the efficiency of GAN-based systems. There are many prior works investigating specialized hardware architectures that can accelerate convolution and deconvolution simultaneously, but they entail intensive hardware modifications to the existing deep learning accelerators like Google TPU and Diannao that focus on convolution acceleration.

In contrast, this work proposes a novel deconvolution layer implementation with a software approach and enables fast and efficient generative network inference on the legacy deep learning processors. Our proposed method reorganizes the computation of deconvolutional layer and allows the deep learning processor to treat it as the standard convolutional layer after we split the original deconvolutional filters into multiple small filters. The proposed data flow is implemented on representative deep learning processors including the dot-production array and the regular 2D PE array architectures. Compared to prior acceleration schemes, the implemented acceleration scheme achieves  $2.41\times$  -  $4.34\times$  performance speedup and reduces the energy consumption by 27.7% - 54.5% on a set of realistic benchmarks. In addition, we also applied the deconvolution computing approach to off-the-shelf commodity deep learning processor chips. The performance of GANs on the Google TPU chip and Intel NCS2 exhibits  $1.67\times$  -  $3.04\times$  speedup on average over prior deconvolution implementations.

## I. INTRODUCTION

Deep neural networks are making continuous breakthroughs in massive research territories over the years. In contrast to early supervised learning paradigms heavily depending on the quality of data labels, GANs [1] have been proved to be superior in a broad domain of content-generation applications and unsupervised learning tasks, because they are able to mimic any distribution of data by learning from a small amount of labeled dataset. Unlike the standard neural networks architectures, GANs are composed of a discriminative model and a generative model. The generative model randomly samples the latent space and learns to generate data for approximation, while the discriminative model distinguishes if the data is synthesized by the generator or from the realistic dataset. The two models compete with each other in a zero-sum game framework and get incrementally optimized towards a stronger discriminator and a generator. Typically, the generator

often involves convolutional layers and also deconvolutional layers for up-sampling. Both layers are compute-intensive and are the performance bottleneck of GANs. Therefore, it is demanded to accelerate the backbone architecture of the GANs, especially the generative networks on end-devices for real-time and low power content generation applications such as real-time deepfake [2] and style transfer [3]. For exemplary GAN benchmarks described in Table I, the deconvolution layers contribute to the major overhead of the multiply-and-add operations in the benchmarked networks (The total operands refer to those of the inference phase). The deconvolution operation is used as an indispensable component to restore the condensed feature maps to full-size at the top of the networks, which are the common architectures in generative networks and other popular models used for semantic segmentation and instance detection [4].

Hardware specialization is a popular approach to accelerate the computation of neural network based applications. To accelerate GANs with customized hardware other than general purpose compute units, researchers have tried a number of approaches from distinct angles. For more efficient design, an intuitive solution is to reuse the convolution processor and build a unified fully convolutional processor for both convolution and deconvolution operations. In such architectures input data of deconvolution can be reorganized by dynamically padding zero activations to the original feature maps and then treat the deconvolution as the conventional convolution layer as presented in Figure 1. Figure 1(a) is an example of the classic deconvolutional operation with the stride of 2, while Figure 1(b) is converted equivalent convolutional operation with stride set to be 1. Eventually, the deconvolution can be mapped to the convolution processor without any hardware modification. However, the zero activations induce considerable redundant computing and degrade the performance of GANs which is illustrated in [5]. Although many CNN accelerators [5]–[10] are able to skip the zero activations during the computing through additional zero detection logic, they typically can only skip a portion of the zero activations especially the ones that are located on the boundary of the feature maps. However, the zero padding deconvolution approach as shown in Figure 1(b) has many zero activations inserted between the non-zero activations and they are usually difficult to be removed due to aligned computing data flow on the parallel computing units in DNN accelerators.

TABLE I  
THE NUMBER OF MULTIPLY-ADD OPERATIONS IN THE INFERENCE PHASE.

Benchmarks	Total operands (M)	Deconvolution operands (M)	%
DCGAN [12]	111.41	109.77	98.5 %
ArtGAN [13]	1268.77	822.08	64.8 %
SNGAN [14]	100.86	100.66	99.8 %
GP-GAN [16]	240.39	103.81	43.2 %
MDE [15]	2638.22	849.35	32.2 %
FST [17]	94730.45	603.98	0.6 %

To improve the computing efficiency of deconvolution, the authors in [11] opted to build independent processor engines for convolution and deconvolution operation respectively. This approach raises a large portion of hardware resources and chip area increase. Different from the above two approaches, the authors in [5] and [12] proposed to revisit the convolutional processor and change the micro-architecture to support both convolution and deconvolution efficiently in a unified processor. In addition, these methods also need dedicated data flow scheduler to make use of the computing engine. For unified architectures, the advantage is better performance and hardware utility, while the disadvantage is the additional redesign and engineering cost. However, for off-the-shelf CNN processors without specialized deconvolution support such as Diannao [7] and TPU [13], the inefficiency and resource under-utilization induced by the zero-padding approach is an inevitable cost to implement the deconvolutional layers.

Inspired by the prior work, we seek to support fast and efficient deconvolution layer implementation on general CNN processors like Eyeriss [6], Diannao [7] and TPU [13], some of which are already commercialized and widely-used in different areas. For these classic CNN processors, many zero-value activations must be padded to the feature map in order to map the deconvolution layers on to them. Instead of zero-padding that induces numerous redundant computing operations, we tailor a novel implementation of deconvolution layer from the software angle, and pre-partition the deconvolutional filters into multiple small convolutional filters, so that the deconvolution operations are converted and can be efficiently implemented on any CNN processor without redesigning or replacing them. In our evaluation on classic CNN processors, the performance as well as the energy efficiency of our deconvolution implementation remains competitive compared to prior work of specialized GAN processors.

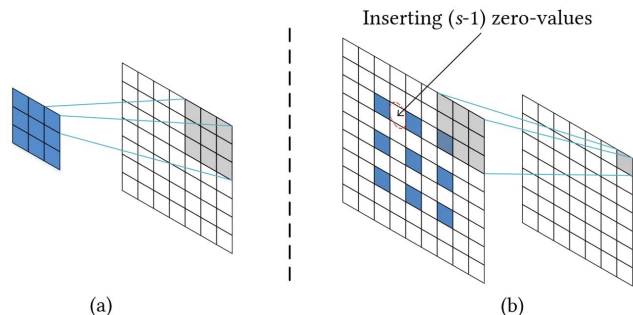


Fig. 1. Computational process of (a) deconvolution and (b) deconvolution with inserted zero-values.

In summary, our contributions are listed as follows:

- We proposed a novel filter partitioning and reorganization approach to convert the deconvolution to standard convolution operations such that the deconvolution can be implemented efficiently on general convolution processor without hardware modification.
- We explored the use of the deconvolution reorganization method on typical CNN processor architectures such as CNN with dot-production/regular 2D computing array and demonstrate the applicability of the method to general CNN processors.
- We evaluated the proposed deconvolution performance on a set of representative benchmarking networks with comprehensive experiments, the experiments show that the proposed approach achieves competitive performance over the state-of-the-art deconvolution processors on both general CNN processors and the most advanced commodity deep learning processor chips such as Google TPU and Intel Neural Compute Stick 2, which are released recently.

The remainder of this paper is organized as follows. Section II presents the related work of deconvolution acceleration design. Section III describes the architecture of typical CNN processors. In Section IV, we elaborate the conversion process of generic split deconvolution in detail. At length, Section V presents the evaluation results and Section VI concludes the paper.

## II. RELATED WORK

With the advancements of deep learning, various neural networks have been proposed to address different tasks such as objection detection and image classification. Among them, GANs are demonstrated to be particularly efficient for content generation tasks such as image style transfer [3], [4], [14] and attracts a lot of attentions. Ledig et al. [15] proposed SRGAN. It adopted a perceptual similarity loss to generate detailed images from low-resolution images. By using GAN, high-resolution images of small objects can be generated and utilized to improve target detection accuracy [16]. GAN can also be applied for sequence data generation as presented in SeqGAN [17] and ORGAN [18]. Additionally, more variants of GANs have been developed and employed in semi-supervised learning and the medical field [19], [20].

However, GANs that consist of both compute-intensive convolution and deconvolution operators cannot be fitted to the conventional CNN processors directly [6]–[8], [21]. While deconvolution is also computing intensive and hinders the acceleration of GANs on CNN processors, thereby, it is highly demanded to explore hardware acceleration of deconvolution operations. Zhang X et al. in [11] proposed to optimize deconvolution with reverse looping and stride hole skipping. Despite the excellent performance, combining independent convolution and deconvolution components in a processor induces considerable chip area and power consumption. Amir Y et al. in [12] proposed to convert deconvolution to convolution by adding zero padding to the activations and then developed a unified MIMD-SIMD processor for both operations. In addition, it implemented a set of distributed on-chip buffers to

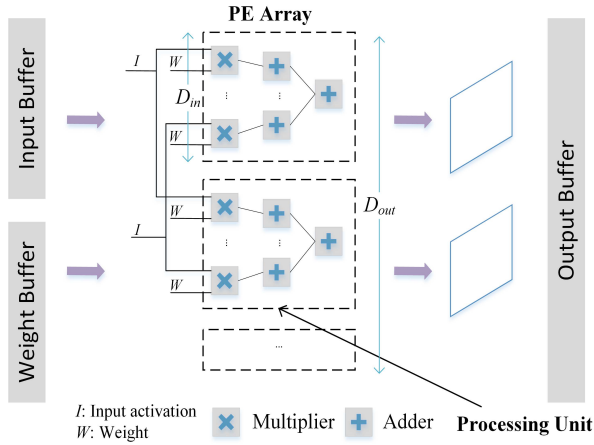


Fig. 2. Dot-production based CNN processor [7]–[10]

avoid the redundant computing brought by the inserted zero activations. Based on [12], the authors further developed an end-to-end template-based solution, which can generate the optimized synthesizable unified processor from a high-level specification of GANs in [22]. Instead of adding zeros to input feature map, Xu et al. in [5] proposed a unified FCN processor on top of a bi-direction systolic array. The FCN processor performs the computing on original input features. The weight and data of adjacent PEs are shared and passed periodically by taking advantage of the small column buffers added to the 2D PE array. Similar to [5], Wang et al. in [23] designed a uniform architecture to support both 2D and 3D deconvolutional neural networks on FPGAs. Multiple FIFOs are added to adjacent PEs to deliver the overlapped temporary results. Yan et al. in [24] proposed a cold buffer to store the overlapped computing results for more efficient data reuse and a novel mapping approach to improve the utilization of the computing array for both convolution and deconvolution. Intel NCS2 [25] also support deconvolution, but there are not much open details. In summary, it can be found that hardware redesigning is typically required to have existing CNN processor to support deconvolution computing in GANs. Due to the long hardware design cycle, many commodity neural network processor including Google Edge TPU [13] and Ropal Neural Compute Stick Lightspeur SPR2801 [26] still do not support the raw GANs yet.

Different from the above works, researchers seek to reuse the conventional CNN processors for GANs without hardware redesigning. Shi et al. [27] presented an example of transformation from deconvolution to convolution by padding zeros to the input feature maps. The zero-padding causes considerable errors because the output feature maps in each layer incur some errors when they are cropped [5] and the errors accumulate across layers of the neural networks. In addition, this work has not gone through the peer review and the experiment is insufficient. Chang et al. [28] utilized filter deformation and proposed an approximate conversion approach targeting at super-resolution image reconstruction problems. While super-resolution image reconstruction can typically tolerate computing errors, the approximate conversion approach works

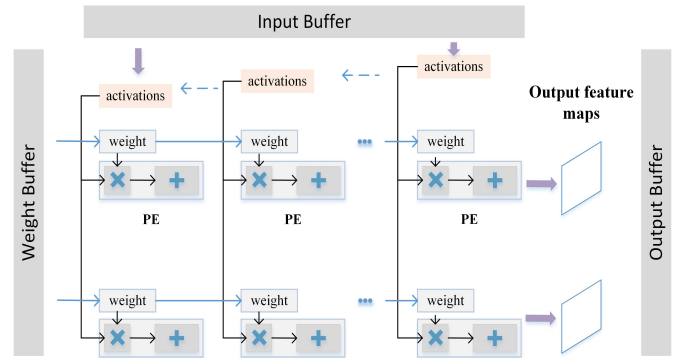


Fig. 3. Regular 2D array CNN processor [5], [6], [13]

fine but it cannot be applied to general GANs that are not necessarily fault-tolerant. In addition, the approach proposed in [28] needs to rearrange the deconvolutional results on CPU instead of CNN processors and it can cause massive data communication between CPU and the processors. To address the above problems, we aim to develop a software approach that can deploy GANs directly on the existing CNN processors without precision penalty nor hardware modification.

### III. TYPICAL CNN PROCESSORS

This section briefly explains the architecture of the two mainstream architectures of general CNN processors assumed in this paper, including dot-production array processor and regular 2D array processor. Most of the prior CNN processors can be included in these two typical architectures [5]–[10], [13].

#### A. Dot-production array processor

Figure 2 shows the dot-production based CNN processor. It consists of  $D_{out}$  neural processing units. Each neural process unit includes  $D_{in}$  multipliers as well as an adder tree and performs a dot production. The same  $D_{in}$  input activations are fed concurrently to each processing unit per cycle while the weights are different. Each unit accepts  $D_{in}$  weights per cycle and  $D_{in} \times D_{out}$  parameters needs to be sent to the array per cycle. In each PE,  $D_{in}$  partial results obtained from multipliers are consumed by the adder tree, and a dot production can be completed each cycle because of the pipelined processing architecture. Once a filter window is processed, the output result is sent to an activation function unit and the result is transferred to the output buffer. Each output activation produced by the processing unit belongs to a different output channel. When weight or data cannot be accommodated by the on-chip buffers, the neural networks will be tiled to fit to the architecture. Dianna [7], Dadianna [8], C-brain [9] and Cnvlutin [10] are typical designs that adopt the dot-production array architecture.

#### B. Regular 2D array processor

Another typical CNN processor architecture with regular 2D PE array is illustrated in Figure 3. Compared to the former structure, it mainly differs on the data flow. The data flow used in this work is output stationary (OS) according to the definition in Eyeriss [6]. Basically, each PE in the

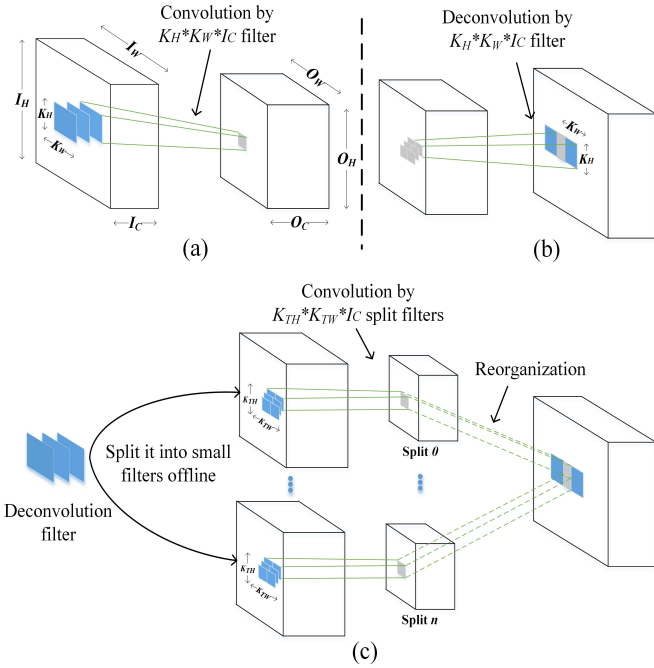


Fig. 4. (a) Convolutional layer (b) Deconvolutional layer (c) Split deconvolution that converts a deconvolution layer to multiple convolution layers

array performs all the operations required to yield an output activation. The weights are fed from the first column of the array and flow across the PEs from left to right to guarantee that all PEs operate in full scale. The input activations are broadcast to all the PEs in a column, but we have at most one PE column to receive the input activations alleviating the pressure on on-chip buffers bandwidth. Each row of the PE array produces output activations of one output feature map on y-axis. Each column PE produces the output activations belonging to different output feature maps but the same pixel positions. Under the circumstances, both input activations and weights consume a limited amount of on-chip memory bandwidth. This architecture enables the proposed system to achieve high reusability and eventually benefits more on boosting throughput in a limited bandwidth provision. This feature is handy in reducing the bandwidth demand caused by weight/activation load and store, especially when the processors are sharing the on-chip storage space and bandwidth with other application processors in nowadays heterogeneous SoCs adopted in mobile and embedded systems. Eyeriss [6], TPU [13], FCN-Engine [5] are typical designs that adopt the 2D array architecture

#### IV. THE PROPOSED SPLIT DECONVOLUTION

In Section IV A, we analyze the correlation between the convolution and deconvolution and brief the idea of converting a deconvolution operation to generic convolutions. Then we present the detailed conversion steps from generic deconvolution operations to standard convolution operations in Section IV B.

#### Algorithm 1 Convolution & Deconvolution

---

**Require:**  $o_h, o_w, o_c, I_C, K_H, K_W$   
**Ensure:**  $output(o_h, o_w, o_c)$

- 1: **function** CONV( $o_h, o_w, o_c, I_C, K_H, K_W$ )
- 2:   **for** ( $i_c = 0; i_c < I_C; i_c ++$ ) **do**
- 3:     **for** ( $k_h = 0; k_h < K_H; k_h ++$ ) **do**
- 4:       **for** ( $k_w = 0; k_w < K_W; k_w ++$ ) **do**
- 5:           $output(o_h, o_w, o_c) += input(o_h \times s + k_h, o_w \times s + k_w, i_c) \times w(k_h, k_w, i_c, o_c)$
- 6: **function** DECONV( $o_h, o_w, o_c, I_C, K_H, K_W$ )
- 7:    $left = \max(0, \text{ceil}((o_w - K_W) / s))$
- 8:    $right = \min(I_W - 1, left + \text{ceil}(K_W / s))$
- 9:    $top = \max(0, \text{ceil}((o_h - K_H) / s))$
- 10:    $bottom = \min(I_H - 1, top + \text{ceil}(K_H / s))$
- 11:   **for** ( $i_c = 0; i_c < I_C; i_c ++$ ) **do**
- 12:     **for** ( $i_h = top; i_h < bottom; i_h ++$ ) **do**
- 13:       **for** ( $i_w = left; i_w < right; i_w ++$ ) **do**
- 14:           $output(o_h, o_w, o_c) += input(i_h, i_w, i_c) \times w(o_h - i_h \times s, o_w - i_w \times s, i_c, o_c)$

---

#### Algorithm 2 Split Deconvolution

---

**Require:**  $o_h, o_w, o_c, I_C, K_H, K_W$   
**Ensure:**  $output(o_h, o_w, o_c)$

- 1: **function** SPLITDECONV( $o_h, o_w, o_c, I_C, K_H, K_W$ )
- 2:   // weights of the  $N$  identical split
- 3:   // convolution:  $w(K_{TH}, K_{TW}, I_C)$
- 4:   **for** ( $n = 0; n < N; n ++$ ) **do**
- 5:     **for** ( $i_c = 0; i_c < I_C; i_c ++$ ) **do**
- 6:        $k_{th} \leftarrow K_{TH} - 1$
- 7:       **for** ( $k_h = \lfloor n/s \rfloor; k_h < K_H; k_h + = s$ ) **do**
- 8:           $k_{tw} \leftarrow K_{TW} - 1$
- 9:          **for** ( $k_w = n \% s; k_w < K_W; k_w + = s$ ) **do**
- 10:            $w(n, k_{th}, k_{tw}, i_c) \leftarrow w(k_h, k_w, i_c)$
- 11:            $k_{tw} \leftarrow k_{tw} - 1$
- 12:            $k_{th} \leftarrow k_{th} - 1$
- 13:        $Conv(o_h^n, o_w^n, o_c^n, I_C, K_{TH}, K_{TW})$
- 14:       Reorganize the obtained  $n$ th output activation

---

#### A. Correlation between Convolution and Deconvolution

Convolution and deconvolution are the major sources of overhead in GANs. Figure 4(a) and 4(b) show the basic computing patterns of the two operations. In convolution i.e. Figure 4(a), windows of input features are convolved with the corresponding filters first. Then the results are added up to obtain an output element of the output feature. In deconvolution i.e. Figure 4(b), each element of the input feature maps is multiplied to each weight matrix first. Then the production in the overlapped position will be accumulated as the final output activation. By definition, convolution and deconvolution is completely different.

In order to reuse the conventional CNN processors for deconvolution operations, we further analyze the computing patterns of convolution and deconvolution. The pseudo code of the two operations for computing one output activation are presented in Algorithm 1. Note that  $I_C$  and  $O_C$  indicate the input and output channel of the feature map.  $I_H$  and  $I_W$  denote the length and width of the input feature map, and  $O_H, O_W$  are the length and width of the output feature map.  $K_H$  and  $K_W$  is the length and width of the filter.  $s$  refers to stride. The notations will be used through this paper. Basically, convolution can be computed with an elementwise approach, while deconvolution is consist of multiple group convolution. Each output activation of convolution i.e.  $output(o_h, o_w, o_c)$  is the accumulation of production of input feature windows



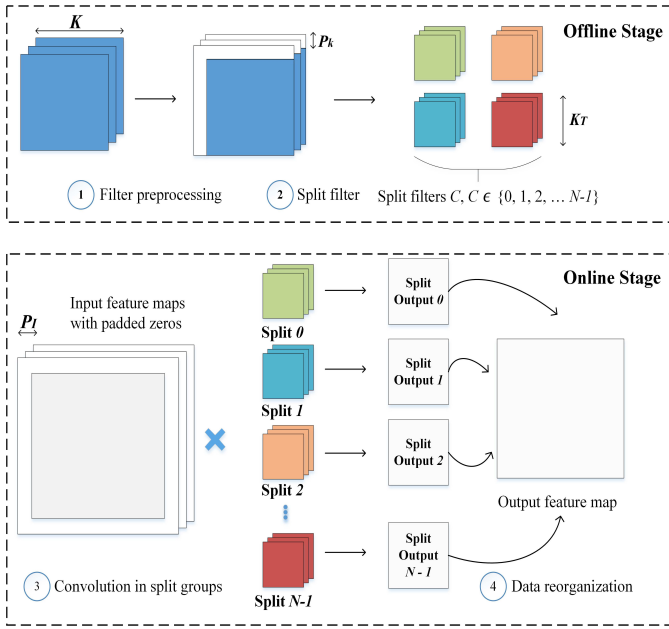


Fig. 5. Conversion steps from deconvolution to convolution, it consists of four steps. 1) The filter is expanded when the filter size is not divisible by the stride. 2) Split the deconvolution filters to multiple small filters according to Equations (4-6). 3) The padded input feature maps convolve with the split filters. 4) Reorganize the split deconvolution results to construct the expected deconvolution output by Equations (10) and (11).

$([o_h \times s, o_h \times s + K_H], [o_w \times s, o_w \times s + K_W])$  with consecutive weight matrices. For deconvolution, each output activation is also the accumulation of production of input feature map window and a set of weights using the same computing function *Convolution* except that the weights are selected with stride  $s$  and reassigned new coordinates in the  $n$ th group. Meanwhile, the output belonging to different groups needs to be reorganized in the final output feature map.

With this observation, we proposed a split deconvolution approach as shown in Algorithm 2 which divides the deconvolution filters into multiple smaller filters with stride  $s$ . In this case, the split filters become consecutive and each deconvolution operation is converted to multiple standard convolution operations. Accordingly, deconvolution can be deployed on conventional CNN processors without any hardware modification. While we need to split the filter and reorganize the obtained activations, detailed conversion approach will be elaborated in the next subsection.

### B. Generic Deconvolution Conversion

Following the above idea, we convert generic deconvolution operation to a set of independent convolution operations. The conversion roughly consists of four steps, as shown in Figure 5.

The first step is the weight preprocessing in which the original deconvolutional filters will be expanded with zeros on the top and left side when its length and width is not divisible by stride  $s$ . It ensures that the deconvolution can be converted to multiple identical convolution operations. The padded zeros will expand the output accordingly while the orientation of the padded zeros guarantees that the center of the expanded output covers the standard deconvolution output. The expanded length

and width  $P_K$  can be calculated with Equation (1) where  $K_T$  is the split filter size (assuming it is square) and can be obtained from Equation (2).

$$P_K = s \times K_T - K \quad (1)$$

$$K_T = \text{ceil}(K / s) \quad (2)$$

The second step is to split the deconvolution filters into multiple small filters with sampling and rotation. Figure 6 illustrates the coordinate distribution of filters before and after the conversion with a small but representative example. To compute an output deconvolution activation with standard convolution operations, filters need to be sampled with stride  $s$  and reorganized into new filters. In addition, each sampled filter needs to be rotated 180 degrees to ensure correct computing. Equation (3) presents the generic conversion. Each deconvolution will be split into  $s^2$  convolution operations. The stride of the split convolution operations is constant 1. Without loss of generality, suppose  $W_n$  is the  $n$ th convolutional filter. It can be obtained with Equation (4-8) where  $W$  is the deconvolution filter,  $(y, x)$  is the original filter coordinate and  $(y_n, x_n)$  is the new coordinate.

$$N = s^2 \quad (3)$$

$$n = s \times \text{mod}(y, s) + \text{mod}(x, s) \quad (4)$$

$$W_n[y_n][x_n] = W[y][x] \quad (5)$$

$$\begin{cases} x_n = K_T - \text{ceil}(x / s) \\ y_n = K_T - \text{ceil}(y / s) \end{cases} \quad (6)$$

where

$$\begin{cases} 0 \leq x < K + P_K \\ 0 \leq y < K + P_K \end{cases} \quad (7)$$

$$\begin{cases} 0 \leq x_n < K_T \\ 0 \leq y_n < K_T \end{cases} \quad (8)$$

$$n \in \{0, 1, 2, \dots, N-1\}$$

Step 1 and Step 2 basically split the deconvolution filters to multiple small convolution filters. This needs to be done only once and can be reused. Therefore, they can be done offline with software approach. Unlike the first two steps, Step 3 and 4 are performed on the CNN processors for each input feature map. In step 3, the input feature maps also need to be padded with zeros to obtain equivalent deconvolution output. Otherwise, the output activations on the edge will be ignored.  $P_I$  columns/rows of zeros will be added where  $P_I$  is obtained from Equation (9).

$$P_I = K_T - 1 \quad (9)$$

Finally, the  $N$  split convolution outputs need to be merged to form the deconvolution output. The reorganization pattern

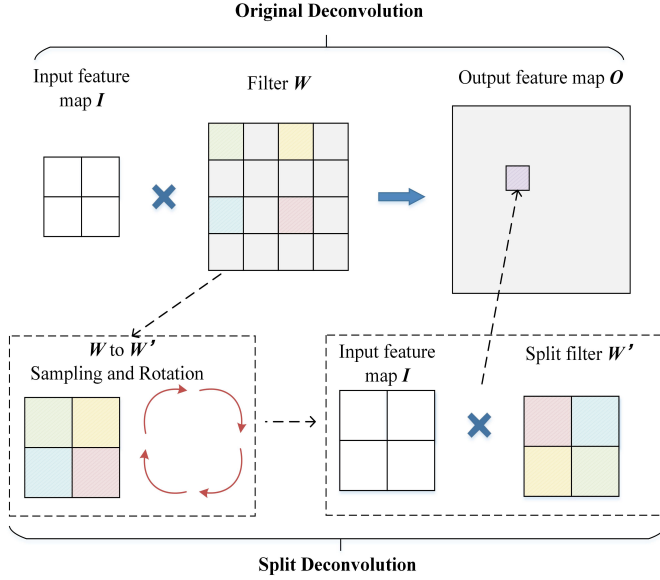


Fig. 6. Weights distribution for an output activation in original deconvolution and split deconvolution where the filter is 4 by 4 and the stride is 2.

is illustrated in Figure 7 and formulated in Equations (10-11). Contrary to the filter splitting process, we pick an element of each convolution output to construct an sAUs window in the deconvolution output. Note that  $ConvO_n[x_i][y_i]$  represents the  $n$ th split convolution output and  $O[x_f][y_f]$  refers to the expected deconvolution output. Suppose  $(y_i, x_i)$  is coordinate of a split convolution output and  $(y_f, x_f)$  is the coordinate of deconvolution output. The reorganization here does not need additional hardware as long as the partial convolution output can write the buffers with stride  $s$  which is usually allowed in generic CNN processors supporting tiling.

$$O[x_f] = ConvO_n[x_i] \times s + \text{mod}(n / s) \quad (10)$$

$$O[y_f] = ConvO_n[y_i] \times s + \text{floor}(n / s) \quad (11)$$

where

$$\begin{cases} 0 \leq x_i < I + 2P_I - K_T + 1 \\ 0 \leq y_i < I + 2P_I - K_T + 1 \end{cases} \quad (12)$$

$$\begin{cases} 0 \leq x_f < (I + 2P_I + 1) \times s + K + P_K \\ 0 \leq y_f < (I + 2P_I + 1) \times s + K + P_K \end{cases} \quad (13)$$

With the above four steps, we can convert generic deconvolution operations to split convolution operations and apply deconvolution on an unmodified CNN processor. In spite of the hardware compatibility, the proposed split deconvolution approach may extend the filters and input feature maps, which will induce additional computing overhead. On the other hand, the padding are zeros and can be potentially skipped by the conventional CNN processor optimizations. Detailed evaluation on realistic benchmarks will be discussed in the experiments.

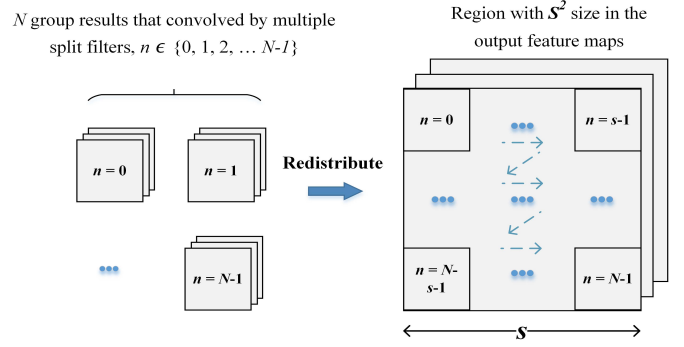


Fig. 7. Demonstrate the redistribution process for multiple groups of output activations.

## V. EVALUATION

This section consists of three parts. First, we listed the setting of the selected benchmarks and the experimental environment. Then we evaluate the performance and energy consumption of split deconvolution on the generic propose processors. At last, the approach is compared with two off-the-shelf processors i.e. Google Edge TPU and Intel NCS2.

### A. Experimental setup

To perform comprehensive evaluation of the proposed split deconvolution computing approach, we conduct experiments on both simulation-based neural network processors and commodity neural network processors provided by the chip vendors, and then compare proposed methods with prior deconvolution computing approaches.

For the simulation-based evaluation, we developed cycle-accurate neural network simulators for both the dot-production based neural network processor architecture and the regular 2D array architecture. Both the 8-bit dot-production PE array and the 2D PE array are implemented and synthesized with Synopsys Design Compiler (DC) under TSMC 65nm library. The dot-production based architecture includes 16 processing units, and each unit performs dot production on 16 input activations and weights. The 2D PE array is set to be 32 by 7. The I/O buffer size is set to be 256 KB, weight buffer is 416 KB. Both processors run at 800 MHz.

For the commodity neural network processors, we choose two representative ones. One of them is Edge TPU [13] from Google and it does not support native deconvolution operations. To implement deconvolution on it, we convert the deconvolution to standard convolution using zero padding [6]. The other processor chip is the latest NCS2 [25] from Intel. It supports native deconvolution operation and the deconvolution is applied directly on the optimized architecture of NCS. The performance on the commodity processors is measured using the system clock.

To evaluate the different deconvolution approaches, we selected a set of advanced neural networks as our benchmarks including ArtGAN [14] on Cifar 10 (ArtGAN), DCGAN [29] on Large-scale CelebFaces Attributes Dataset (DCGAN), Spectral Normalization for GAN [30] on Cifar 10 (SNGAN), GP-GAN on Transient Attributes Database [31] (GP-GAN) for generating new datasets. Unsupervised Monocular Depth

Estimation of FCN on KITTI and Cityscapes [4] (MDE) aims of image segmentation, and Fast-Style-Transfer [3] on CoCo2014 which is used to apply the style of one image to another image (FST).

### B. Experimental results on general CNN processors

This section illustrates how the proposed split deconvolution improves the performance and efficiency of GANs on the simulated general CNN processors including both dot-production array and 2D array architectures.

1) **Operation number comparison:** Multiply-add (MAC) operation takes up the majority of the computing in neural networks, so the number of MACs exhibits the computing intensity of the neural networks directly and it is independent with the underlying computing architectures. Thereby, we use this metric to compare the different deconvolution computing approaches. Table II shows the number of MACs in original neural networks, neural networks using native zero padding (NZIP) and neural networks using the proposed split deconvolution (SD). It can be observed that NZP incurs a large number of redundant computations compared with the original deconvolution. Compared to NZP, SD brings in much less computing. It does not incur any additional computing overhead in SNGAN, ArtGAN and GP-GAN and induces only a portion of additional computing on the rest of the neural networks.

In theory, SD will not increase the amount of the computation, but there are occasions that zeros need to be added for more efficient computing on processors. When the original filter length or width is not divisible by the stride  $s$  in the according neural networks, we need to pad zeros on the top and left side of the filters to ensure identical filter splitting. In addition, the split deconvolution may produce only the center area of the original deconvolution output feature maps, and we must add zero paddings to the input feature maps to obtain equivalent deconvolution output feature maps. Thereby, the proposed split deconvolution may add zeros to both the weights and the input activations, and induce more computing depending on the neural network parameters.

2) **Performance comparison:** In this section, we mainly compare the different deconvolution approaches on typical neural network processors. Although NZP and SD may induce redundant computing, many of the redundant computing can be potentially squeezed using the sparse aware optimization techniques which allow the processors to skip the zero multiplications. Generally, there are three different sparse-aware

TABLE II  
COMPARISON OF MULTIPLY-ADD OPERANDS (DECONVOLUTION LAYERS)  
FOR THREE DIFFERENT IMPLEMENTATIONS

Benchmarks	Original Deconvolution (M)	Native Zero-padding Deconvolution (M)	Split Deconvolution (M)
DCGAN [12]	109.77	439.09	158.07
ArtGAN [13]	822.08	2030.04	822.08
SNGAN [14]	100.66	402.65	100.66
GP-GAN [16]	103.81	415.23	103.81
MDE [15]	849.347	3397.39	1509.95
FST [17]	603.98	2415.92	1073.74

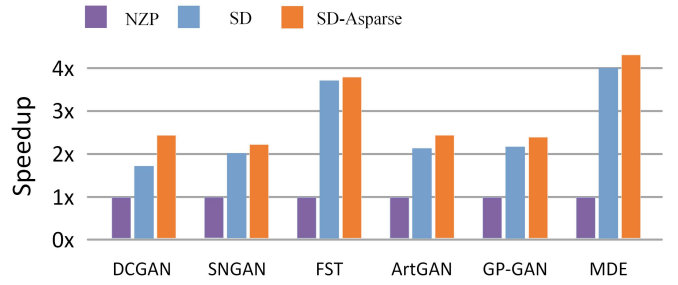


Fig. 8. Performance comparison of the deconvolutional layers in the dot-production PE array.

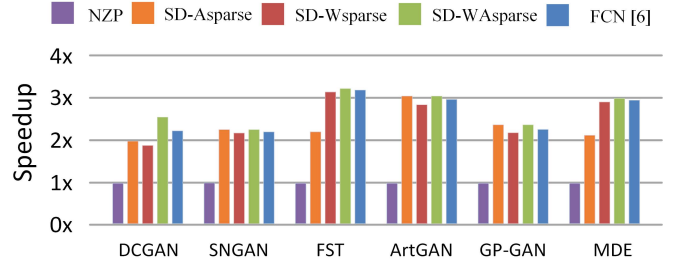


Fig. 9. Performance comparison of the deconvolutional layers in the regular 2D PE array.

optimization methods including activation sparse optimization (Asparse), weight sparse optimization (Wsparse) and activation and weight sparse optimization (AWsparse). We explored the neural network performance on processors with the different optimization methods. While the processor with dot-production PE array cannot skip zero weights and we only apply Asparse method on it. In addition, we also compare with FCN-engine [5] that had the 2D PE array CNN processor redesigned.

Figure 8 depicts the normalized performance of three acceleration schemes on the dot-production PE array. NZP incurs 75% computing redundancy on average on the benchmark neural networks when converting the deconvolution to convolution. Unlike the NZP, split deconvolution has only marginal zero paddings on the boundary in some corner cases. Therefore, it has much less computing redundancy, which is projected in the 2.5 $\times$  performance boost of SD over NZP. When the specified input activation lines can be skipped to generate standard deconvolution output, the performance can further be improved. Notably, SD-Asparse on DCGAN improves by 1.4 $\times$ . The primary reason lies in the fact that the DCGAN has fewer network layers and smaller input feature maps. As a result, the computing redundancy caused by the padding affects the overall performance more significantly.

On the 2D PE array CNN processor as shown in Figure 9, SD-Asparse and SD-Wsparse in the experiments show the influence of the filter expansion and the input expansion respectively. Although SD-Wsparse induces some redundant computation due to padding to the input feature maps, most of the convolution processors support zero-skipping and can squeeze the computing redundancy automatically. Compared to SD-Wsparse, SD-WAsparse that enables the zero-skipping reduces 22% redundant computation on average. Similarly,

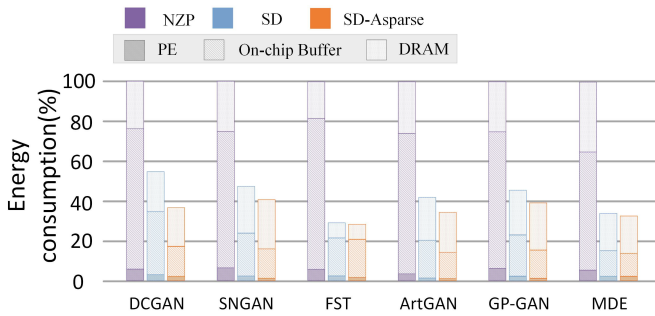


Fig. 10. Energy consumption of the deconvolutional layers in the dot-production PE array.

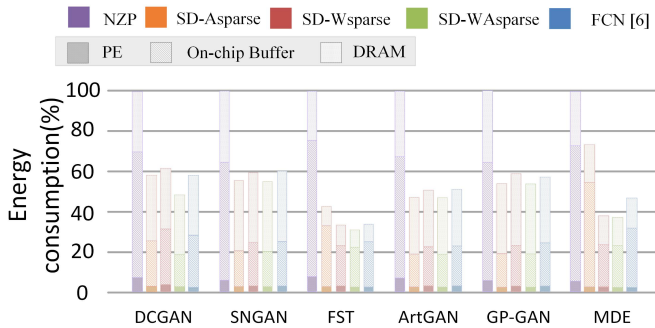


Fig. 11. Energy consumption of the deconvolutional layers in the regular 2D PE array.

SD-Asparse has zero-padding added to the weights, and the redundant computing can also be eliminated on a sparse convolution processor architecture. For workloads like DCGAN, FST, and MDE, the filters need to be expanded. In these cases, SD-WAsparse reduces 75% - 80% computing redundancy with zero-skipping. When the split deconvolution is deployed on optimized CNN processors, the performance of SD-WAsparse is on par with that of FCN in all the benchmark neural networks. The deconvolution approach presented in FCN-engine [6] adopts a bi-directional data flow. It has implemented the original deconvolution, which is the input activations multiplied with each filter and then accumulates the overlapped production. By taking advantage of the column buffers, it can transmit the partial results for accumulation efficiently. However, the output feature maps on edge are redundant and need to be cropped, which inevitably induces computing overhead, especially for smaller deconvolution layers. Therefore, SD-WAsparse outperforms FCN-engine on some of the neural networks like DCGAN, as shown in Figure 9.

3) **Energy consumption comparison:** Figures 10 and 11 present the relative energy consumption distribution of the different deconvolution approaches on the dot-production PE array and regular 2D PE array respectively. Compared to NZP, the average energy consumption of SD-Asparse and SD-WAsparse reduce by 36.15% and 43.63% respectively on the two CNN architectures. Unlike the performance comparison, the energy consumption comparison is less significant. In general, the deconvolution energy consumption roughly consists of three parts i.e. PE, on-chip buffer, and DRAM. According to the estimation using CACTI [32], the energy

TABLE III  
SSIM VALUE COMPARED WITH STANDARD OUTPUT

Benchmarks	Larger Output	Shi [7]	Chang [9]
DCGAN [12]	1	0.534	0.568
FST [17]	0.989	0.939	0.742

is mostly consumed by the DRAM access and the on-chip buffer access. While the amount of DRAM access of the different deconvolution approaches is about the same, their consumption has little difference across these approaches. Despite the dramatic difference in PE activity and energy consumption, PE energy consumption is too small to affect the overall deconvolution energy consumption. As a result, the energy consumption difference is primarily determined by the amount of on-chip buffer access, which explains all the energy consumption difference. For example, SD-Asparse induces relatively more weight reading and thus higher energy consumption. Similarly, FCN requires additional on-chip buffers to support the unified convolution and deconvolution, so the overall energy consumption is higher than that of SD-WAsparse in all the benchmark networks, though their performance is quite close to each other.

4) **Application analysis:** Some of the CNN processors may not be able to discard part of the output activations and generate the expanded output in split deconvolution and the approaches of [27] and [28] lack versatility for generic GANs which generate unprecise results, we further evaluate the generated images of these three circumstances on two real applications using SSIM metric [33] which is widely used to measure similarity between images. One of them is a typical generative task using DCGAN and the other one is a fast style transfer network. For split deconvolution, the expanded output feature map will not lose any information based on DCGAN. In contrast, the generated images from [27] and [28] are structurally different from the original, as shown by SSIM metric in Table III. In the application of fast style transfer (FST), the SSIM is 0.989 of expanded output since there are instance normalization layers [34] in the networks, the expanded output feature map will lead to different computing result. Even so, the images we generated are still superior to others in image similarity.

### C. Experiments on commodity NN processors

This section shows how the proposed split deconvolution improves the performance and efficiency of GANs on the most advanced commodity CNN processor chips including Google Edge TPU without specialized deconvolution support and Intel NCS2 with optimized deconvolution operators in hardware.

1) **Edge TPU:** Edge TPU is a tensor processor with the systolic array architecture and is usually used as a coprocessor of a host computer. It does not support native deconvolution operation, so we apply the NZP approach to implement the deconvolution on it as the baseline. Meanwhile, we also perform split deconvolution (SD) to deploy deconvolution on TPU. The NZP approach requires zero-padding to the input feature maps, and the SD approach needs additional output feature reorganization. While this computing cannot be performed on TPU



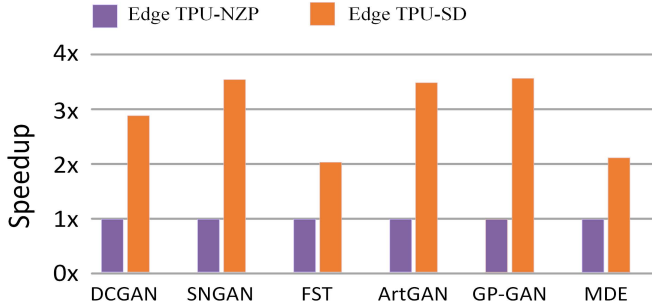


Fig. 12. Performance comparison on Edge TPU.

directly, we have them done on the host processor. We have all the additional computing and corresponding data movement taken into consideration during the runtime measurement to make a fair end-to-end performance comparison.

The normalized acceleration performance of the two deconvolution approaches on Edge TPU is illustrated in Figure 12. The proposed SD achieves  $3.04\times$  performance speedup over NZP on average, which is roughly consistent with the magnitude of operation reduction presented in Table II. Particularly, the performance speedup goes up to  $3.60\times$  on GP-GAN. Similar to Figure 9, the average performance improvement of DCGAN, FST, and MDE is relatively lower than that of SNGAN, ArtGAN, and GPGAN due to the additional parameters padded to the filters and the input features during splitting.

2) *Intel Neural Compute Stick 2 (NCS2)*: NCS2 is a neural network processor produced by Intel, and it includes specialized hardware to support native deconvolution operation. We evaluated the deconvolutional layers of GANs on it with the deconvolution operations implemented using the NZP approach, the SD approach as well as the native deconvolution. The experiment is presented in Figure 13. When compared to NZP, the proposed SD performs  $1.67\times$  performance speedup over the NZP approach, which is much lower than that on Edge TPU and is not consistent with the number of operations as listed in Table II. To explore the underlying reasons, we further evaluate the computing efficiency of convolution with different input feature map sizes and filter sizes on NCS2. The evaluation result is revealed in Table IV and Table V. The filter size is set to be  $3\times 3$ , which is a frequent setup for split deconvolution and measure the Giga multiply-add operations per second (GMACPS) given different input feature maps. As shown in Table IV, when the size of input feature maps ranges from  $8\times 8$  to  $128\times 128$ , the normalized computational efficiency of NCS2 i.e. GMACPS increases significantly. Although there are not much documents about the detailed computing architecture of NCS2, it is probably that NCS2 parallelizes the convolution operations on the 2-D plane of the input features and requires larger input feature maps to make good use of its computing resources. Similarly, we also investigate the influence of filter sizes on the computing efficiency in Table V. We set the feature map to be  $128\times 128$  and change the filter size from  $2\times 2$  to  $5\times 5$ . When we compare the computing efficiency, it can be observed that the convolution with larger filter sizes on NCS2 is clearly more efficient. For SD that splits the deconvolution

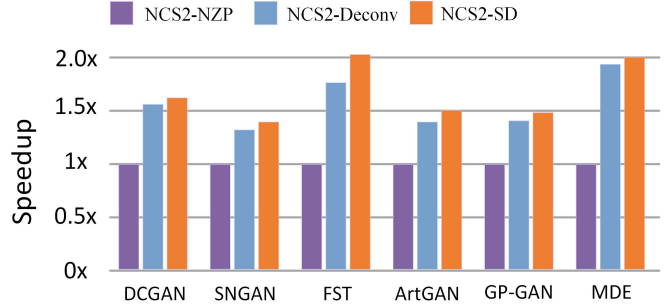


Fig. 13. Performance comparison on Intel Neural Compute Stick 2.

operations to multiple smaller convolution operations, the resulting convolution is usually less efficient compared to the NZP based converter. Basically, the computing efficiency of NCS2 degrades with smaller feature maps and filter sizes due to its inherent convolution parallelization approach. Thereby, the performance speedup of SD over NZP is lower than that is estimated based on the number of MACs.

NCS2 also includes specialized hardware for native deconvolution operation. We evaluated the deconvolutional layers of GANs on it with the native deconvolution. Even compared to the native deconvolution implementation approach on NCS2, the proposed SD approach still yields  $1.10\times$  performance speedup on average. It demonstrates that the proposed SD approach is able to make good use of the computing resources in the deep learning processors without any hardware modification.

## VI. CONCLUSION

Deconvolution is a critical computing-intensive operation in GANs that have been widely deployed in many generative tasks. Unlike prior deconvolution acceleration works which may either require intensive hardware modification of existing CNN processors or bring in large amount of redundant computing, we proposed a novel software approach to convert the deconvolution to multiple standard convolution such that the deconvolution can be accelerated efficiently on legacy CNN processors without hardware modification. Basically, we

TABLE IV  
NORMALIZED GMACPS FOR DIFFERENT INPUT FEATURE MAP SIZE

Feature map size	# of input channels	# of output channels	Normalized GMACPS
$8\times 8$	256	128	1x
$16\times 16$	256	128	4.55x
$32\times 32$	256	128	10.70x
$64\times 64$	256	128	14.71x
$128\times 128$	256	128	15.45x

TABLE V  
NORMALIZED GMACPS FOR DIFFERENT FILTER SIZE

Filter Size	# of input channels	# of output channels	Normalized GMACPS
$2\times 2$	256	128	1x
$3\times 3$	256	128	2.14x
$4\times 4$	256	128	3.64x
$5\times 5$	256	128	5.22x

split the original deconvolution filters into multiple smaller filters. Afterwards, we can perform the convolution with the split filters on input feature data and recombine the produced multigroup split feature maps online. With comprehensive experiments, we demonstrate the proposed split deconvolution approach on both a dot-product PE array and regular 2D PE array. The split deconvolution achieves  $2.41 \times$  and  $4.34 \times$  performance speedup over the naïve zero padding methods and is on par with the prior optimized implementation on modified fully convolution neural network processor. In addition, the proposed approach is also beneficial to commodity neural network processors. When we apply it to the Edge TPU and Intel NCS2 chips, the resulting performance of GANs achieves  $3.04 \times$  and  $1.67 \times$  speedup on average respectively compared to that using the zero padding-based implementations. For Intel NCS2 that has specialized hardware acceleration for GANs, the proposed software approach still achieves  $1.10 \times$  performance speedup.

## REFERENCES

- [1] I. Goodfellow, J. Pouget-Abadie, M. Mirza, B. Xu, D. Warde-Farley, S. Ozair, A. Courville, and Y. Bengio, "Generative adversarial nets," in *Advances in neural information processing systems*, 2014, pp. 2672–2680.
- [2] I. Korshunova, W. Shi, J. Dambre, and L. Theis, "Fast face-swap using convolutional neural networks," in *Proceedings of the IEEE International Conference on Computer Vision*, 2017, pp. 3677–3685.
- [3] L. Engstrom, "Fast style transfer," <https://github.com/lengstrom/fast-style-transfer/>, 2016.
- [4] C. Godard, O. Mac Aodha, and G. J. Brostow, "Unsupervised monocular depth estimation with left-right consistency," in *Proceedings of the IEEE Conference on Computer Vision and Pattern Recognition*, 2017, pp. 270–279.
- [5] D. Xu, K. Tu, Y. Wang, C. Liu, B. He, and H. Li, "Fcn-engine: Accelerating deconvolutional layers in classic cnn processors," in *Proceedings of the International Conference on Computer-Aided Design*. ACM, 2018, p. 22.
- [6] Y.-H. Chen, J. Emer, and V. Sze, "Eyeriss: A spatial architecture for energy-efficient dataflow for convolutional neural networks," in *ACM SIGARCH Computer Architecture News*, vol. 44, no. 3. IEEE Press, 2016, pp. 367–379.
- [7] T. Chen, Z. Du, N. Sun, J. Wang, C. Wu, Y. Chen, and O. Temam, "Diannao: A small-footprint high-throughput accelerator for ubiquitous machine-learning," in *ACM Sigplan Notices*, vol. 49, no. 4. ACM, 2014, pp. 269–284.
- [8] Y. Chen, T. Luo, S. Liu, S. Zhang, L. He, J. Wang, L. Li, T. Chen, Z. Xu, N. Sun *et al.*, "Dadiannao: A machine-learning supercomputer," in *Proceedings of the 47th Annual IEEE/ACM International Symposium on Microarchitecture*. IEEE Computer Society, 2014, pp. 609–622.
- [9] L. Song, Y. Wang, Y. Han, X. Zhao, B. Liu, and X. Li, "C-brain: A deep learning accelerator that tames the diversity of cnns through adaptive data-level parallelization," in *2016 53rd ACM/EDAC/IEEE Design Automation Conference (DAC)*. IEEE, 2016, pp. 1–6.
- [10] J. Albericio, P. Judd, T. Hetherington, T. Aamodt, N. E. Jerger, and A. Moshovos, "Cnvlutin: Ineffectual-neuron-free deep neural network computing," *ACM SIGARCH Computer Architecture News*, vol. 44, no. 3, pp. 1–13, 2016.
- [11] X. Zhang, S. Das, O. Neopane, and K. Kreutz-Delgado, "A design methodology for efficient implementation of deconvolutional neural networks on an fpga," *arXiv preprint arXiv:1705.02583*, 2017.
- [12] A. Yazdanbakhsh, K. Samadi, N. S. Kim, and H. Esmailzadeh, "Ganax: A unified mimd-simd acceleration for generative adversarial networks," in *Proceedings of the 45th Annual International Symposium on Computer Architecture*. IEEE Press, 2018, pp. 650–661.
- [13] N. P. Jouppi, C. Young, N. Patil, D. Patterson, G. Agrawal, R. Bajwa, S. Bates, S. Bhatia, N. Boden, A. Borchers *et al.*, "In-datacenter performance analysis of a tensor processing unit," in *2017 ACM/IEEE 44th Annual International Symposium on Computer Architecture (ISCA)*. IEEE, 2017, pp. 1–12.
- [14] W. R. Tan, C. S. Chan, H. E. Aguirre, and K. Tanaka, "Artgan: Artwork synthesis with conditional categorical gans," in *2017 IEEE International Conference on Image Processing (ICIP)*. IEEE, 2017, pp. 3760–3764.
- [15] C. Ledig, L. Theis, F. Huszár, J. Caballero, A. Cunningham, A. Acosta, A. Aitken, A. Tejani, J. Totz, Z. Wang *et al.*, "Photo-realistic single image super-resolution using a generative adversarial network," in *Proceedings of the IEEE conference on computer vision and pattern recognition*, 2017, pp. 4681–4690.
- [16] J. Li, X. Liang, Y. Wei, T. Xu, J. Feng, and S. Yan, "Perceptual generative adversarial networks for small object detection," in *Proceedings of the IEEE Conference on Computer Vision and Pattern Recognition*, 2017, pp. 1222–1230.
- [17] L. Yu, W. Zhang, J. Wang, and Y. Yu, "Seqgan: Sequence generative adversarial nets with policy gradient," in *Thirty-First AAAI Conference on Artificial Intelligence*, 2017.
- [18] G. L. Guimaraes, B. Sanchez-Lengeling, C. Outeiral, P. L. C. Farias, and A. Aspuru-Guzik, "Objective-reinforced generative adversarial networks (organ) for sequence generation models," *arXiv preprint arXiv:1705.10843*, 2017.
- [19] L. Chongxuan, T. Xu, J. Zhu, and B. Zhang, "Triple generative adversarial nets," in *Advances in neural information processing systems*, 2017, pp. 4088–4098.
- [20] D. Yang, T. Xiong, D. Xu, Q. Huang, D. Liu, S. K. Zhou, Z. Xu, J. Park, M. Chen, T. D. Tran *et al.*, "Automatic vertebra labeling in large-scale 3d ct using deep image-to-image network with message passing and sparsity regularization," in *International Conference on Information Processing in Medical Imaging*. Springer, 2017, pp. 633–644.
- [21] Y. Wang, J. Xu, Y. Han, H. Li, and X. Li, "Deepburning: automatic generation of fpga-based learning accelerators for the neural network family," in *Proceedings of the 53rd Annual Design Automation Conference*. ACM, 2016, p. 110.
- [22] A. Yazdanbakhsh, M. Brzozowski, B. Khaleghi, S. Ghodrati, K. Samadi, N. S. Kim, and H. Esmailzadeh, "Flexigan: An end-to-end solution for fpga acceleration of generative adversarial networks," in *2018 IEEE 26th Annual International Symposium on Field-Programmable Custom Computing Machines (FCCM)*. IEEE, 2018, pp. 65–72.
- [23] D. Wang, J. Shen, M. Wen, and C. Zhang, "Towards a uniform architecture for the efficient implementation of 2d and 3d deconvolutional neural networks on fpgas," in *2019 IEEE International Symposium on Circuits and Systems (ISCAS)*. IEEE, 2019, pp. 1–5.
- [24] J. Yan, S. Yin, F. Tu, L. Liu, and S. Wei, "Gna: Reconfigurable and efficient architecture for generative network acceleration," *IEEE Transactions on Computer-Aided Design of Integrated Circuits and Systems*, vol. 37, no. 11, pp. 2519–2529, 2018.
- [25] "Intel neural compute stick 2," <https://software.intel.com/en-us/neural-compute-stick>.
- [26] "Ropal neural compute stick, lightspeur spr2801," <https://www.ropal.com.cn/>.
- [27] W. Shi, J. Caballero, L. Theis, F. Huszar, A. Aitken, C. Ledig, and Z. Wang, "Is the deconvolution layer the same as a convolutional layer?" *arXiv preprint arXiv:1609.07009*, 2016.
- [28] J.-W. Chang and S.-J. Kang, "Optimizing fpga-based convolutional neural networks accelerator for image super-resolution," in *Proceedings of the 23rd Asia and South Pacific Design Automation Conference*. IEEE Press, 2018, pp. 343–348.
- [29] A. Radford, L. Metz, and S. Chintala, "Unsupervised representation learning with deep convolutional generative adversarial networks," *arXiv preprint arXiv:1511.06434*, 2015.
- [30] T. Miyato, T. Kataoka, M. Koyama, and Y. Yoshida, "Spectral normalization for generative adversarial networks," *arXiv preprint arXiv:1802.05957*, 2018.
- [31] H. Wu, S. Zheng, J. Zhang, and K. Huang, "Gp-gan: Towards realistic high-resolution image blending," *arXiv preprint arXiv:1703.07195*, 2017.
- [32] S. Li, K. Chen, J. H. Ahn, J. B. Brockman, and N. P. Jouppi, "Cacti-p: Architecture-level modeling for sram-based structures with advanced leakage reduction techniques," in *Proceedings of the International Conference on Computer-Aided Design*. IEEE Press, 2011, pp. 694–701.
- [33] Z. Wang, A. C. Bovik, H. R. Sheikh, E. P. Simoncelli *et al.*, "Image quality assessment: from error visibility to structural similarity," *IEEE transactions on image processing*, vol. 13, no. 4, pp. 600–612, 2004.
- [34] D. Ulyanov, A. Vedaldi, and V. Lempitsky, "Instance normalization: The missing ingredient for fast stylization," *arXiv preprint arXiv:1607.08022*, 2016.